Supplemental Document

optica

Nondissipative non-Hermitian dynamics and exceptional points in coupled optical parametric oscillators: supplement

ARKADEV ROY,[1] SAMAN JAHANI,[1] QIUSHI GUO,[1] AVIK DUTT,[2] SHANHUI FAN,[2] MOHAMMAD-ALI MIRI,[3] AND ALIREZA MARANDI[1,*]

[1] *Department of Electrical Engineering, California Institute of Technology, Pasadena, California 91125, USA*
[2] *E. L. Ginzton Laboratory, Stanford University, Stanford, California 94305, USA*
[3] *Department of Physics, Queens College, City University of New York, New York, New York 11367, USA*
[*] *Corresponding author: marandi@caltech.edu*

Supplement DOI: https://doi.org/10.6084/m9.figshare.13772917

Parent Article DOI: https://doi.org/10.1364/OPTICA.415569

Non-Dissipative Non-Hermitian Dynamics and Exceptional Points in Coupled Optical Parametric Oscillators: supplemental document

1. THRESHOLD

The threshold for parametric oscillation can be obtained from the linearized analysis.

Threshold for degenerate oscillation occurs when the following equality is satisfied:

$$-\gamma + \frac{1}{\sqrt{2}}\sqrt{f^2 + g^2 - 2\kappa^2 + \sqrt{f^4 + g^4 - 4g^2\kappa^2 - 4f^2\kappa^2 - 2g^2f^2 + 8\kappa^2 fgcos(\phi)}} = 0 \tag{S1}$$

Threshold for non-degenerate oscillation occurs when the following equality is satisfied:

$$-\gamma + \max\left[\mathbf{Im}(E_+), \mathbf{Im}(E_-)\right] = 0 \tag{S2a}$$

where,

$$E_\pm = \pm\frac{1}{\sqrt{2}}\sqrt{2\kappa^2 - f^2 - g^2 - \sqrt{f^4 + g^4 - 4g^2\kappa^2 - 4f^2\kappa^2 - 2g^2f^2 + 8\kappa^2 fgcos(\phi)}} \tag{S2b}$$

provided, $\mathbf{Re}(E) \neq 0$.

Below the oscillation threshold the linearized analysis determines the system dynamics and the properties can be accessed experimentally by probing it with a tunable laser.

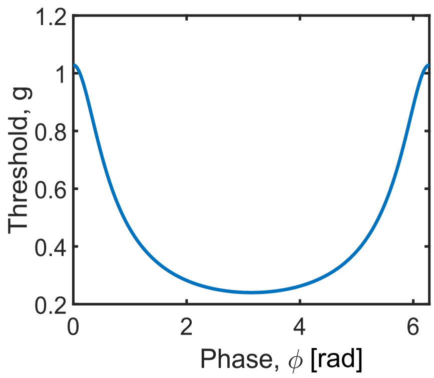

Fig. S1. Threshold as a function of the phase difference ϕ between the pumps. The curve is obtained using Eq(S.2) which matches with that of the numerical simulation.

2. NONLINEARITY INDUCED PHASE TRANSITION

We analytically demonstrate the phenomenon of nonlinearity induced phase transition in a simple case although a representative one, when $f = g$ and $\phi = \pi$. The linearized analysis suggests that the system of coupled OPO's under this set of condition will oscillate in the non-degenerate regime. However, we find that beyond a critical g the system oscillates in degenerate mode.

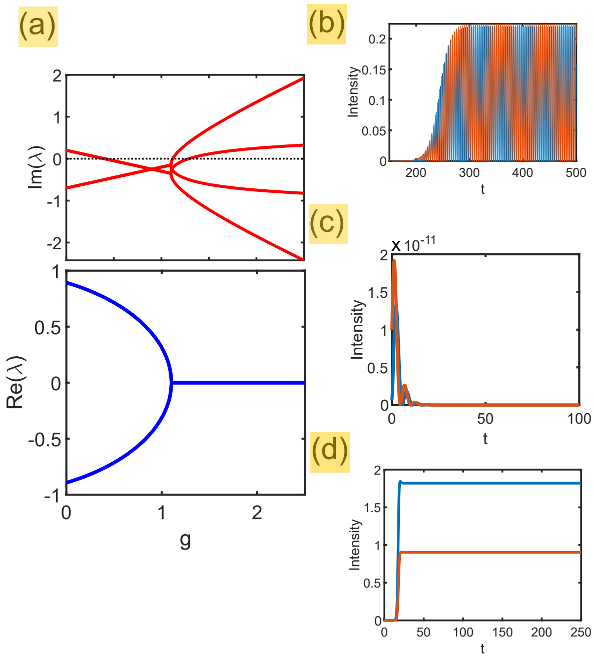

Fig. S2. Gain induced oscillation suppression and revival of oscillation. a) Eigenvalues from linear analysis. Parameters used are: $f = 0.9, \gamma = 0.25, \kappa = 1$. b) Coupled OPO above threshold and oscillating in the non-degenerate phase for $g = 0.3$ c) Oscillation is suppressed as the gain is increased to $g = 0.75$ indicating the occurrence of gain induced oscillation suppression. d) Oscillation again re-emerges as the gain parameter is further increased ($g = 1.5$), signifying the revival of oscillation.

Under this set of conditions when the system oscillates in the degenerate mode beyond a critical g, the signal envelopes can be assumed as: $a = x$ and $b = i\rho x$, where ρ determines the intensity contrast in the two resonators at steady state, and x is real. Substituting this ansatz in Eq(1) of the main text, we obtain at steady state:

$$G - g_s x^2 - \kappa\rho = 0 \tag{S3a}$$

$$G\rho - g_s \rho^3 x^2 + \kappa = 0 \tag{S3b}$$

where, G= g-γ. Solving these system of equations yields:

$$x = \frac{1}{\sqrt{g_s}}\sqrt{\frac{3G}{4} + \frac{\sqrt{G^2 - 8\kappa^2}}{4} + \frac{\kappa}{2}\sqrt{2 + \frac{G^2}{2\kappa^2} - \kappa\frac{\frac{G^3}{\kappa^3} - \frac{8G}{\kappa}}{2\sqrt{G^2 - 8\kappa^2}}}} \tag{S3c}$$

$$\rho = \frac{G}{4\kappa} - \frac{\sqrt{G^2 - 8\kappa^2}}{4\kappa} - \frac{1}{2}\sqrt{2 + \frac{G^2}{2\kappa^2} - \kappa\frac{\frac{G^3}{\kappa^3} - \frac{8G}{\kappa}}{2\sqrt{G^2 - 8\kappa^2}}} \tag{S3d}$$

The critical value of g beyond which the oscillation enters into degenerate regime is given by: $g = \gamma + \sqrt{8\kappa^2}$. This analytical results matches with the critical value of g obtained numerically.

3. HIGHER ORDER EXCEPTIONAL POINT

Here, we derive the conditions to obtain the family of higher order (fourth-order) exceptional points.

$$(\lambda_R + i\lambda_I)\begin{bmatrix} A \\ B^* \\ C \\ D^* \end{bmatrix} = \begin{bmatrix} -i\gamma - \Delta & ig & -\kappa & 0 \\ ig & -i\gamma + \Delta & 0 & \kappa \\ -\kappa & 0 & -i\gamma & img \\ 0 & \kappa & img & -i\gamma \end{bmatrix}\begin{bmatrix} A \\ B^* \\ C \\ D^* \end{bmatrix} \tag{S4a}$$

$$g = \sqrt{\frac{-\kappa^2}{m^3} + \frac{\kappa^2}{m^2} + \frac{\sqrt{\kappa^4 m^2 (1 - 2m + 2m^2)}}{m^4}} \tag{S4b}$$

$$\Delta = \pm\sqrt{-\kappa^2 - \frac{\kappa^2}{m^3} + \frac{\kappa^2}{m^2} - \frac{\kappa^2}{m} + \frac{\sqrt{\kappa^4 m^2 (1 - 2m + 2m^2)}}{m^4} + \frac{\sqrt{\kappa^4 m^2 (1 - 2m + 2m^2)}}{m^2}} \tag{S4c}$$

with, $m \neq \{0, 1\}$.

4. FLOQUET CONTROL OF EXCEPTIONAL POINT

We show the time domain and frequency domain picture of the Floquet modulated parametric non-Hermitian system in Fig. S3. The Floquet phase diagram is shown in Fig. S4.

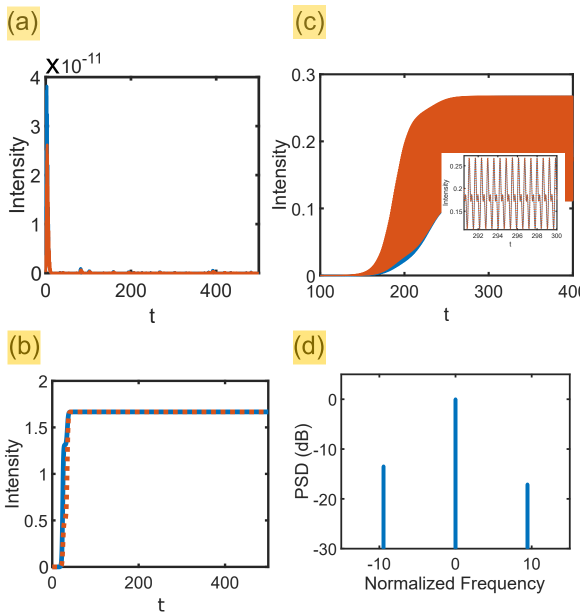

Fig. S3. Floquet control of EP. Parameters used for the amplitude modulation are $F = 5, \omega = 10$. a) System of coupled OPO below threshold for $g_0 = 1.25$. The time domain intra-cavity intensity waveforms are shown. b) However in the absence of periodic modulation i.e. $F = 0$, the system oscillates above threshold in the degenerate phase. This demonstrates that the Floquet control can tune the exceptional point and thereby the oscillation threshold. c) The modulated Floquet system goes above threshold for $g_0 = 1.3$.The time domain intra-cavity intensity waveforms are shown. d) Spectral domain representation for the waveforms in c, depicting the presence of sidebands at the modulating frequency.

5. FIXED POINTS OF COUPLED OPO

We plot the steady-state fixed point solutions of the quadratures of coupled OPO in Fig. S5 and Fig. S6.

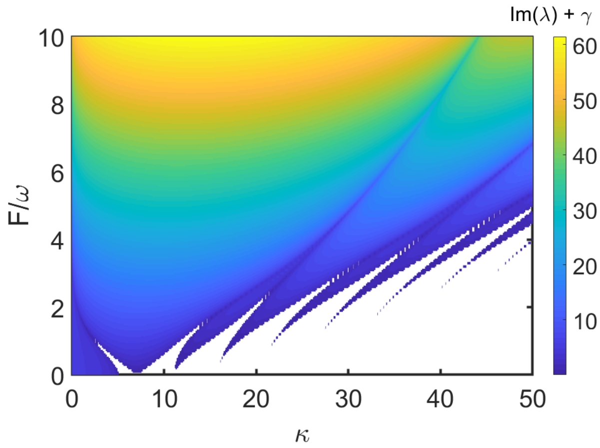

Fig. S4. Floquet phase diagram. Multiple regions of below and above threshold regions (related to the anti-PT symmetry breaking) reflecting the usual resonance like behavior of periodically modulated systems. Plotted is the imaginary part of the eigenvalue shifted by the constant loss (γ). Here, the modulation amplitude F and the coupling factor κ is varied, with $\omega = 10$.

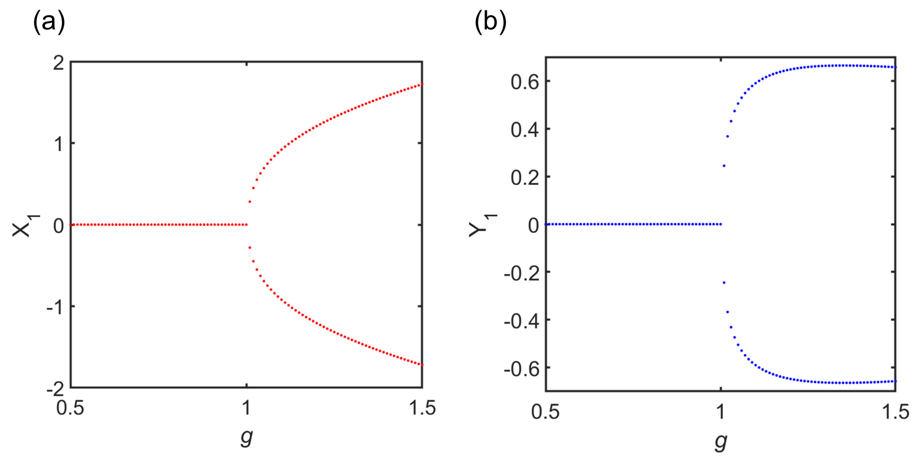

Fig. S5. Steady states appearing as stable fixed points for the coupled OPO system when the gain parameter is varied. It displays features of a super-critical bifurcation at threshold. Plotted are the quadratures of the complex field of one OPO in the coupled OPO system.

6. COUPLED OPO BELOW THRESHOLD: QUANTUM LANGEVIN EQUATIONS

Here we develop the input-output formalism of the coupled OPO for analysis of the quantum behavior. This formalism has been used to obtain the results of the Quantum Regime subsection of the Results section of the main text.

The signal fields $\hat{a}$ and $\hat{b}$ in the resonators constituting the OPO's experience a roundtrip loss (γ) consisting of two contributons: out-coupling loss (μ) and round-trip propagation loss (α). We define (ρ) as, $\rho = \frac{\mu}{\gamma}$, which is the ratio between out-coupling and total loss. The OPO operates below threshold. Also the pump is non-resonant and the pumps driving the OPO's are not coupled to each other. So we can adiabatically eliminate the pump dynamics and represent the pump field with a coherent field.

The effective Hamiltonian in the rotating frame is given by: $H = H_{int} + H_{coup}$ which is comprised of the nonlinear interaction Hamiltonian and the conservative coupling Hamiltonian. We assume that both the OPO's are driven by identical pump since we are interested in exploring the quantum behaviour as we approach the exceptional point from below threshold.

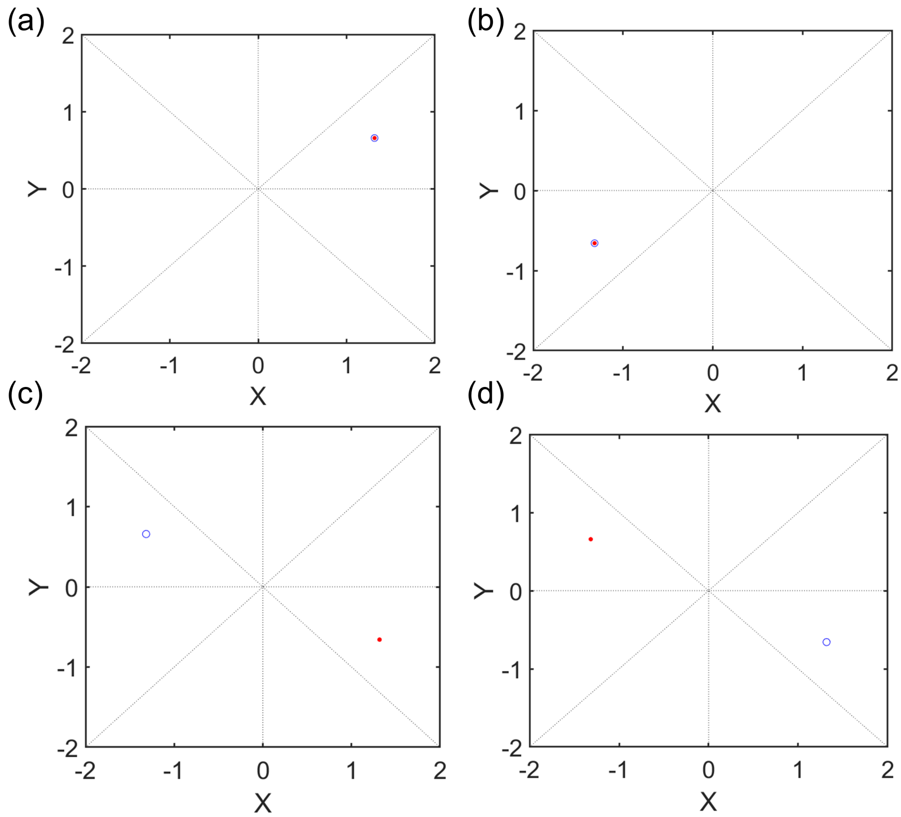

Fig. S6. Multiple steady states appearing as stable fixed points for the coupled OPO system above threshold. The parameters involved are: $f = g = 1.25, \gamma = 0.1, \kappa = 1$, and $g_s = 0.3$. These steady states have different in-phase and out-of phase quadrature components. They can be accessed with suitable initial condition lying in their domain of attraction.Red filled circles represent the field in the first OPO, while open blue circles represent the same for the second OPO. Dotted lines depict X=0, Y=0, Y=X, and Y=-X.

$H_{int} = \frac{i\hbar}{2}\left[g(\hat{a}^{\dagger})^2 - g^*(\hat{a})^2 + g(\hat{b}^{\dagger})^2 - g^*(\hat{b})^2\right]$ and $H_{coup} = \hbar\kappa\left[\hat{a}\hat{b}^{\dagger} + \hat{b}\hat{a}^{\dagger}\right]$.

We include the loss arising from different mechanisms and the accompanying fluctuations ($\hat{V}$) using the input-output formalism of open quantum systems. We can write the Heisenberg-Langevin equations for the intra-cavity field as [1]:

$$\dot{\hat{a}} = -\gamma\hat{a} + g\hat{a}^{\dagger} + i\kappa\hat{b} + \sqrt{2\alpha}\hat{V}_{\alpha,a} + \sqrt{2\mu}\hat{V}_{\mu,a} \tag{S5a}$$

$$\dot{\hat{b}} = -\gamma\hat{b} + g\hat{b}^{\dagger} + i\kappa\hat{a} + \sqrt{2\alpha}\hat{V}_{\alpha,b} + \sqrt{2\mu}\hat{V}_{\mu,b} \tag{S5b}$$

The respective output field can be mapped to the intra-cavity field as:

$$\hat{A}_{out} = \sqrt{2\mu}\hat{a} - \hat{V}_{\mu,a} \tag{S5c}$$

$$\hat{B}_{out} = \sqrt{2\mu}\hat{b} - \hat{V}_{\mu,b} \tag{S5d}$$

We assume that the fluctuations have zero mean field and is delta-correlated Gaussian noise sources. Noise from independent channels are non-correlated. These fluctuations which provides the Langevin forces follow the following commutation relations:

$$\begin{gathered}\left\langle \hat{V}_{l,j}(t)\hat{V}^{\dagger}_{l'j'}(t')\right\rangle = \delta_{ll'}\delta_{jj'}\delta(t-t') \\ \left\langle \hat{V}^{\dagger}_{l,j}(t)\hat{V}_{l'j'}(t')\right\rangle = \left\langle \hat{V}_{l,j}(t)\hat{V}_{l'j'}(t')\right\rangle = \left\langle \hat{V}^{\dagger}_{l,j}(t)\hat{V}^{\dagger}_{l'j'}(t')\right\rangle = 0\end{gathered} \tag{S6a}$$

where $l \in \{\mu, \alpha\}$ and $j \in \{a, b\}$. We define the fourier transform as: $\tilde{V}(\omega) = \frac{1}{\sqrt{2\pi}} \int_{-\infty}^{\infty} dt \hat{V}(t) e^{i\omega t}$. Therefore in the spectral domain the noise correlations appear as:

$$\begin{gathered} \left\langle \tilde{V}_{l,j}(\omega) \tilde{V}^{\dagger}_{l',j'}(\omega') \right\rangle = \delta_{ll'} \delta_{jj'} \delta(\omega - \omega') \\ \left\langle \tilde{V}^{\dagger}_{l,j}(\omega) \tilde{V}_{l',j'}(\omega') \right\rangle = \left\langle \tilde{V}_{l,j}(\omega) \tilde{V}_{l',j'}(\omega') \right\rangle = \left\langle \tilde{V}^{\dagger}_{l,j}(\omega) \tilde{V}^{\dagger}_{l',j'}(\omega') \right\rangle = 0 \end{gathered} \tag{S6b}$$

We define the amplitude and phase quadratures as follows: $\hat{X}_1 = \hat{a} + \hat{a}^{\dagger}, \hat{X}_2 = \hat{b} + \hat{b}^{\dagger}, \hat{Y}_1 = -i\left(\hat{a} - \hat{a}^{\dagger}\right)$,and $\hat{Y}_2 = -i\left(\hat{b} - \hat{b}^{\dagger}\right)$.

Below threshold, the mean values of the fields are zero. The fluctuations of the quadratures can be studied by analyzing the following linearized dynamics:

$$\begin{bmatrix} \dot{\hat{X}}_1 \\ \hat{X}_2 \\ \hat{Y}_1 \\ \hat{Y}_2 \end{bmatrix} = J \begin{bmatrix} \hat{X}_1 \\ \hat{X}_2 \\ \hat{Y}_1 \\ \hat{Y}_2 \end{bmatrix} + \sqrt{2\alpha} \begin{bmatrix} \hat{W}^{\alpha}_{1,0} \\ \hat{W}^{\alpha}_{2,0} \\ \hat{W}^{\alpha}_{1,\pi/2} \\ \hat{W}^{\alpha}_{2,\pi/2} \end{bmatrix} + \sqrt{2\mu} \begin{bmatrix} \hat{W}^{\mu}_{1,0} \\ \hat{W}^{\mu}_{2,0} \\ \hat{W}^{\mu}_{1,\pi/2} \\ \hat{W}^{\mu}_{2,\pi/2} \end{bmatrix} \tag{S7}$$

where,

$$J = \begin{bmatrix} -\gamma + g & 0 & 0 & -\kappa \\ 0 & -\gamma + g & -\kappa & 0 \\ 0 & \kappa & -\gamma - g & 0 \\ \kappa & 0 & 0 & -\gamma - g \end{bmatrix} \tag{S8}$$

and, $\hat{W}^{l}_{j,0} = \hat{V}_{l,j} + \hat{V}^{\dagger}_{l,j}$, $\hat{W}^{l}_{j,\pi/2} = -i\left(\hat{V}_{l,j} - \hat{V}^{\dagger}_{l,j}\right)$, $l \in \{\mu, \alpha\}$ and $j \in \{a, b\}$. The respective output field can be mapped to the intra-cavity field as:

$$\begin{bmatrix} \hat{X}_{1,out} \\ \hat{X}_{2,out} \\ \hat{Y}_{1,out} \\ \hat{Y}_{2,out} \end{bmatrix} = \sqrt{2\mu} \begin{bmatrix} \hat{X}_1 \\ \hat{X}_2 \\ \hat{Y}_1 \\ \hat{Y}_2 \end{bmatrix} - \begin{bmatrix} \hat{W}^{\mu}_{1,0} \\ \hat{W}^{\mu}_{2,0} \\ \hat{W}^{\mu}_{1,\pi/2} \\ \hat{W}^{\mu}_{2,\pi/2} \end{bmatrix} \tag{S9}$$

In the spectral domain we get,

$$\begin{bmatrix} \tilde{X}_{1,out}(\omega) \\ \tilde{X}_{2,out}(\omega) \\ \tilde{Y}_{1,out}(\omega) \\ \tilde{Y}_{2,out}(\omega) \end{bmatrix} = -\sqrt{2\mu}\left[J + i\omega I_4\right]^{-1} \left(\sqrt{2\alpha} \begin{bmatrix} \hat{W}^{\alpha}_{1,0}(\omega) \\ \hat{W}^{\alpha}_{2,0}(\omega) \\ \hat{W}^{\alpha}_{1,\pi/2}(\omega) \\ \hat{W}^{\alpha}_{2,\pi/2}(\omega) \end{bmatrix} + \sqrt{2\mu} \begin{bmatrix} \hat{W}^{\mu}_{1,0}(\omega) \\ \hat{W}^{\mu}_{2,0}(\omega) \\ \hat{W}^{\mu}_{1,\pi/2}(\omega) \\ \hat{W}^{\mu}_{2,\pi/2}(\omega) \end{bmatrix} \right) - \begin{bmatrix} \hat{W}^{\mu}_{1,0}(\omega) \\ \hat{W}^{\mu}_{2,0}(\omega) \\ \hat{W}^{\mu}_{1,\pi/2}(\omega) \\ \hat{W}^{\mu}_{2,\pi/2}(\omega) \end{bmatrix} \tag{S10}$$

I_4 is an identity matrix of order 4. The output correlation matrix can be written as:

$$C^{out}(\omega) = \int_{-\infty}^{\infty} d\omega' \left\langle \begin{bmatrix} \tilde{X}_{1,out}(\omega) \\ \tilde{X}_{2,out}(\omega) \\ \tilde{Y}_{1,out}(\omega) \\ \tilde{Y}_{2,out}(\omega) \end{bmatrix} \begin{bmatrix} \tilde{X}_{1,out}(\omega') \\ \tilde{X}_{2,out}(\omega') \\ \tilde{Y}_{1,out}(\omega') \\ \tilde{Y}_{2,out}(\omega') \end{bmatrix}^{T} \right\rangle \tag{S11}$$

where T stands for matrix transpose operation.

$$C^{out}(\omega) = \left(2\mu\left[J + i\omega I_4\right]^{-1} + I_4\right) C^{in}(\omega) \left(2\mu\left[J - i\omega I_4\right]^{-1} + I_4\right)^{T} + 4\mu\alpha\left(J + i\omega I_4\right)^{-1} C^{in}(\omega) \left(\left(J - i\omega I_4\right)^{-1}\right)^{T} \tag{S12}$$

The input correlation matrix is:

$$C^{in}(\omega) = \begin{bmatrix} I_2 & iI_2 \\ -iI_2 & I_2 \end{bmatrix} \tag{S13}$$

I_2 is an identity matrix of order 2.

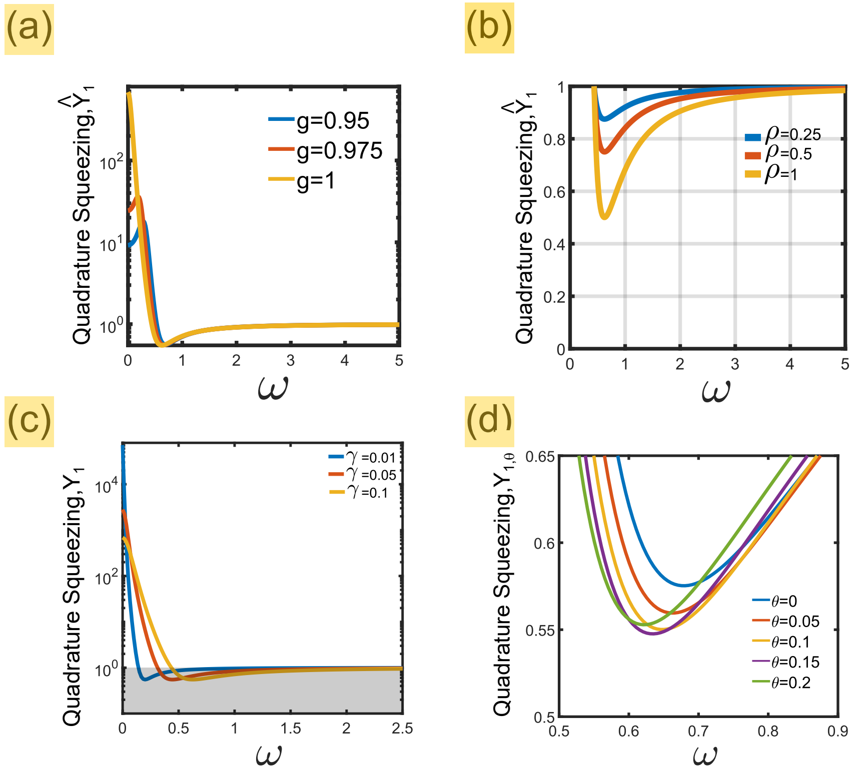

Fig. S7. Quadrature squeezing near EP. a) The squeezing spectrum is plotted in log scale. The quadrature variance at DC diverges as we approach the exceptional point. Parameters used are: $f = g, \gamma = 0.1, \kappa = 1$, and $\rho = 0.9$. b) Squeezing spectrum as the parameter ρ is varied. Best squeezing performance is ideally obtained for $\rho = 1$. c) Divergence of the variance (PSD) at DC for different values of total round-trip loss γ. $\rho = 0.9$ is kept constant. d) Rotation of the optimum quadrature for squeezing. Parameters used are $f = g = 1, \gamma = 0.1, \rho = 0.9$, and $\Delta_1 = 0.1$. θ are measured in radians.

7. 3 DB QUADRATURE SQUEEZING LIMIT IN THE VICINITY OF EP IN COUPLED OPO

The squeezing spectrum for the quadrature ($\hat{Y}$), is obtained from (Eq S.12) as $S(\omega) = C^{out}_{3,3}$. We are interested in the squeezing that is achievable at the EP. Assuming, $\kappa = 1$ and $g = \kappa$ (EP), we get:

$$S(\omega) = \frac{\gamma^4 - 4\gamma^3\rho - 4\gamma\rho\omega^2 + \omega^4 + 2\gamma^2(4\rho + \omega^2)}{(\gamma^2 + \omega^2)^2} \tag{S14}$$

Maximum, squeezing is obtained in the limit, $\rho = 1$. The function $S(\omega)$ reaches its minimum at $\omega = \sqrt{4\gamma - \gamma 2}$, if $0 \leq \gamma \leq 4$. The maximum attainable squeezing is 3dB below the shot noise level. If $\gamma > 4$, the minimum is obtained at $\omega = 0$.

Various aspects of the quadrature squeezing near the exceptional point is shown in Fig. S7.

8. QUANTUM FISHER INFORMATION: BOUNDS TO PARAMETER ESTIMATION

Let, the parameter to be estimated is θ, which can be the cavity detuning perturbation. If the cavity detuning perturbation is applied to the first cavity mode, then the perturbed Jacobian can be written as:

$$J_\theta = \begin{bmatrix} -\gamma + g & 0 & -\theta & -\kappa \\ 0 & -\gamma + g & -\kappa & 0 \\ \theta & \kappa & -\gamma - g & 0 \\ \kappa & 0 & 0 & -\gamma - g \end{bmatrix} \tag{S15}$$

We consider that the output of the system of coupled OPO when probed with an input state will be Gaussian. The output state can then be fully characterized by the mean (μ_θ) and Variance (V_θ). Clearly, the mean and variance will be a function of the perturbation parameter θ. Our goal is to infer the parameter θ, by measuring the output state. We won't be able to obtain the exact value of θ, but rather an estimate of it, given by $\hat{\theta}$. If our estimator is unbiased, then in the limit of N measurements ($N \to \infty$), the mean value will approach the true value. The goodness of the estimator is determined by the standard deviation $\delta\theta$, which can achieve a minimum value governed by the Fisher information from detection and estimation theory, and is well known as the Cramer-Rao bound: $\delta\theta \geq \frac{1}{\sqrt{N}\sqrt{I_{FI}}}$, where N is the number of observations and I_{FI} is the Fisher information metric. Thus Fisher information provides the lower bound from a single measurement and dictates the limit of precision of a sensing protocol.

While Fisher information deals with the precision limit of a given sensing protocol, the Quantum Fisher information provides the ultimate precision limit considering all possible measurement protocols. The Quantum Fisher information (QFI) for Gaussian states can be approximated as [2, 3]:

$$I_{QFI} \sim \left(\frac{d\mu_\theta}{d\theta}\right)^T V_\theta^{-1} \left(\frac{d\mu_\theta}{d\theta}\right) + \frac{1}{2} Tr \left[V_\theta^{-1} \left(\frac{dV_\theta}{d\theta}\right) V_\theta^{-1} \left(\frac{dV_\theta}{d\theta}\right)\right] \tag{S16}$$

where, μ_θ and V_θ denotes the mean and covariance of the quadratures.μ_θ can be expressed as: $\mu_\theta = -(\sqrt{2\mu}(J_\theta - \mathrm{i}\omega I_4)^{-1} + I_4)\mu_{in}$, where μ_{in} is the excitation probe quadrature amplitude vector. The covariance matrix V_θ can be obtained using (Eq. S12) with J replaced by J_θ .

The optimum achievable SNR then scales as SNR $\sim \theta^2 I_{QFI}$. Fig. S8 shows the scaling of quantum Fisher information when the sensor is operated at or in the vicinity of the parametric EP. The green shaded regime in Fig. S8(a) indicates the range of perturbation where EP enhanced favourable scaling is obtained. In this regime, the EP based sensor can exhibit better precision than its diabolic point based Hermitian counterparts as shown in Fig. S8(b). The sharp resonance like feature appearing in the plots indicates very large precision. But this may also suggest that in that neighbourhood the linearized treatment based on which our formalism is developed may not be valid in that case, and a nonlinear treatment may be required. It is clear that the QFI is a smooth function of gain parameter as EP is approached ($\theta = 0$). So, although there can be a advantage of using EP based sensor for the parameter space corresponding to the green shaded region, the precision is not diverging/ dramatic/ exceptional at EP.

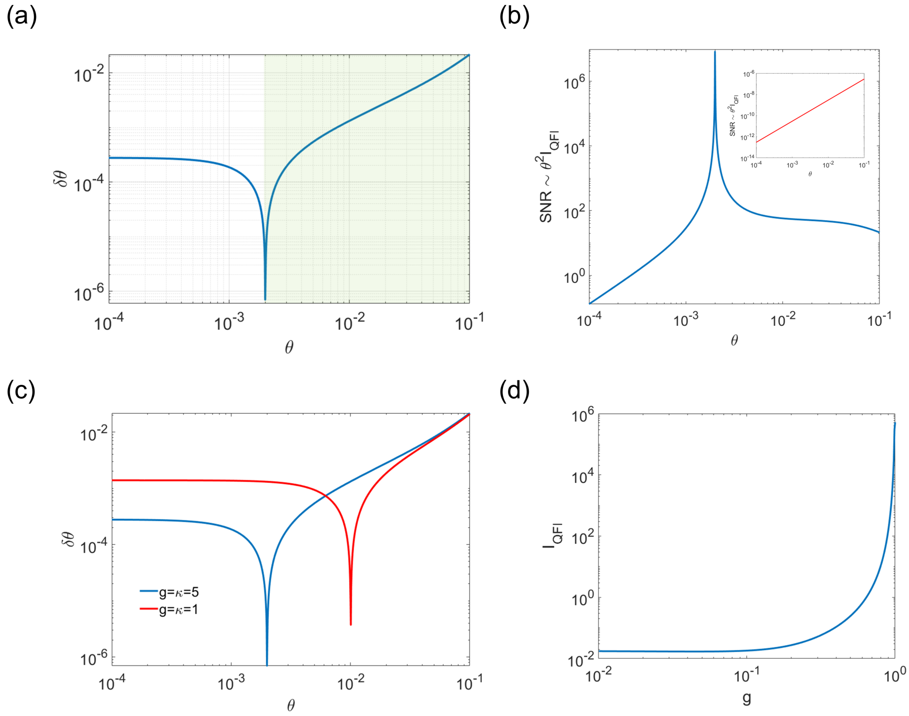

Fig. S8. Quantum Fisher information near parametric EP. a) Standard deviation of the estimator ($\delta\theta$) as a function of the perturbation (θ) as given by the quantum Cramer-Rao bound. The green shaded region highlights the regime of perturbation where EP enhanced sensor can have favourable scaling. The parameters used in the simulation are: $\gamma = 0.1, \kappa = g = 5$. b) SNR calculated using QFI shows EP based sensor reaching a maximum as opposed to Hermitian sensor based on diabolic point which shows a θ^2 scaling as shown in the inset. . c) Effect of varying the loss parameter with respect to the coupling and gain parameters. The blue curve corresponds to $\gamma = 0.1, \kappa = g = 5$, while the red curve corresponds to $\gamma = 0.1, \kappa = g = 1$. d) Dependence of the QFI as the EP is approached. Here $\theta = 0$ is assumed and $\gamma = 0.1, \kappa = 1$. In obtaining the results all quadratures have been equally excited.

9. OPO GOVERNING EQUATION: CLASSICAL MEAN-FIELD REGIME

We model the OPO using a simplified governing equation which takes into account the parametric gain and the gain saturation (due to second harmonic generation of the signal back to the pump). We assume the OPO to operate at degeneracy. The parametric oscillation occurs in a high Q cavity, and is oscillating in a CW mode.

A. Non-resonant pump configuration

The quadratic nonlinear interaction happening in the phase matched $\chi^{(2)}$ region is given by:

$$\frac{da}{dz} = \epsilon b a^* \tag{S17a}$$

$$\frac{db}{dz} = -\frac{\epsilon}{2} a^2 \tag{S17b}$$

where, a and b represents the signal and pump fields respectively. ϵ is the effective nonlinear co-efficient. Let, L be the length of the nonlinear interaction region. In the high Q limit, we can assume that the field does not change significantly within a round-trip. So, Eq (S.17) can be expressed in the n^{th} round-trip as:

$$b_n = b_0 - \frac{\epsilon}{2} L a_n^2 \tag{S18}$$

where, b_0 is the input pump. So, we can express the evolution of the signal field on a round-trip basis as:

$$a_{n+1} = a_n + \epsilon b_0 L a_n^* - \frac{1}{2}\epsilon^2 L^2 |a_n|^2 a_n \tag{S19}$$

The loss in each round-trip can be included as:

$$a_{n+1} = a_n e^{-\gamma T} \tag{S20}$$

The detuning in each round-trip can be included as:

$$a_{n+1} = a_n e^{\mathrm{i}\Delta T} \tag{S21}$$

where, ΔT is the total detuning per round-trip. where, γ is the loss per unit time, and T is the round-trip time. In the high Q limit, we can convert the difference equation in a differential form as:

$$T\frac{da}{dt} = -\gamma T a + \mathrm{i}\Delta T a + \epsilon b_0 L a^* - \frac{1}{2}\epsilon^2 L^2 |a|^2 a \tag{S22}$$

This reduces to:

$$\frac{da}{dt} = -\gamma a + \mathrm{i}\Delta a + \epsilon b_0 \frac{L}{T} a^* - \frac{1}{2T}\epsilon^2 L^2 |a|^2 a \tag{S23}$$

Thus, we define $g = \epsilon b_0 \frac{L}{T}$ which denotes the parametric gain, and $g_s = \frac{1}{2T}\epsilon^2 L^2$ which denotes the gain saturation co-efficient.

B. OPO with resonant pump where adiabatic elimination is valid i.e. ($\gamma_p >> \gamma_s$)

We consider the case, where the pump is also resonant, but the time scales are drastically different such that we can perform the adiabatic elimination. Let the loss rates corresponding to the signal and pump be represented by γ_s and γ_p respectively. In the limit, $\gamma_p >> \gamma_s$ the adiabatic elimination is valid. The evolution equation of the signal and pump can then be given by:

$$\frac{da}{dt} = -\gamma_s a + \mathrm{i}\Delta_s a + \epsilon b a^* \tag{S24a}$$

$$\frac{db}{dt} = -\gamma_p a + \mathrm{i}\Delta_p b - \frac{1}{2}\epsilon a^2 + b_0 \tag{S24b}$$

Solving the pump field after performing adiabatic elimination we get:

$$b = \frac{b_0 - \frac{1}{2}\epsilon a^2}{\gamma_p + \mathrm{i}\Delta_p} \tag{S25}$$

Substituting this back into Eq S.24a we get:

$$\frac{da}{dt} = -\gamma_s a + \mathrm{i}\Delta_s a + \frac{\epsilon b_0}{\gamma_p + \mathrm{i}\Delta_p} a^* - \frac{\epsilon^2}{2}\frac{\gamma_p - \mathrm{i}\Delta_p}{\gamma_p^2 + \Delta_p^2}|a|^2 a \tag{S26}$$

In the case of $\Delta_p = 0$, we obtain the simplified model as given by Eq S.23.

REFERENCES

1. Y. K. Chembo, "Quantum dynamics of Kerr optical frequency combs below and above threshold: Spontaneous four-wave mixing, entanglement, and squeezed states of light," Phys. Rev. A **93**, 033820 (2016).
2. H.-K. Lau and A. A. Clerk, "Fundamental limits and non-reciprocal approaches in non-Hermitian quantum sensing," Nat. Commun. **9**, 1–13 (2018).
3. L. Banchi, S. L. Braunstein, and S. Pirandola, "Quantum fidelity for arbitrary Gaussian states," Phys. Rev. Lett. **115**, 260501 (2015).